

In Situ Compressive Sensing

Lawrence Carin, Dehong Liu, and Bin Guo
Department of Electrical and Computer Engineering
Duke University
Durham, NC 27708-0291
{lcarin,liudh,bg25}@ece.duke.edu

Abstract

Compressive sensing (CS) is a framework that exploits the compressible character of most natural signals, allowing the accurate measurement of an m -dimensional signal u in terms of $n \ll m$ measurements v . The CS measurements may be represented in terms of an $n \times m$ matrix that defines the linear relationship between v and u . In this paper we demonstrate that similar linear mappings of the form $u \rightarrow v$ are manifested naturally by wave propagation in general media, and therefore *in situ* CS measurements may be performed simply by exploiting the propagation and scattering properties of natural environments. The connection between the propagation medium and the basis in which u is sparsely rendered is quantified in terms of a mutual-coherence factor, which plays an important role in defining the number of required *in situ* CS measurements. In addition to presenting the basic *in situ* CS framework, a simple but practical example problem is considered in detail from multiple perspectives.

I. INTRODUCTION

In the 1990s significant research was performed on the compact representation of natural signals, images and video, with this having important consequences in the context of modern digital signal processing and compression. An important example of this research is the wavelet transform [1], [2]. From a practical standpoint, one of the key observations is that most natural signals are highly compressible in a wavelet basis; this implies that, when performing a wavelet transform of a natural signal, most wavelet coefficients may be discarded with minimal impact on the accuracy of the reconstructed signal. As a consequence of this, most modern compression standards, for both images and video, are now wavelet-based [3], [4]. The complexity of such compression

schemes is that, while most natural signals are compressible in a wavelet basis, the specific wavelet coefficients that may be discarded are dependent on the distinct signal under test. Consequently, the compression algorithm must adapt to each signal of interest [3], [4].

While the impact of such compression schemes has been profound, there are some limitations worthy of further consideration. Specifically, in a practical system m components of a signal are measured, with analog-to-digital (A/D) converters applied to each component (*e.g.*, pixel), and then after compression (effectively) $n \ll m$ transform coefficients are retained. Given the complexity of many A/D converters, and potentially because of the time and energy resources required to measure the m signal components, one may ask whether the informative part of the signal (that part retained after conventional compression) may be measured more directly. This question has spawned the field of compressive sensing (CS) [5]–[10].

In CS, rather than directly measuring the signal u , one measures a signal v which is a linear combination of the components of u . For a wide class of such linear relationships between u and v , one may recover u accurately based on a relatively small number of CS measurements; the inverse mapping $v \rightarrow u$ is effectively regularized by exploiting the fact that u is compressible (with linkages to ℓ_1 regularization [11]). Remarkably, the linear projections used to map u to v (and hence perform the CS measurements) are non-adaptive; *i.e.*, the same CS measurements are performed for all signals of interest (*vis-à-vis* traditional transform coding which, as discussed above, must adapt to the signal under test).

The CS framework summarized above has motivated design of a new class of sensors. For example, rather than performing digital-picture measurements with numerous pixels, as in traditional digital cameras, a single-pixel CS camera has been demonstrated [12], [13]. Similar ideas are being explored in the context of magnetic-resonance imaging (MRI) [14].

With this understanding, one may now consider a separate line of research that has been explored in other fields. Specifically, in phase conjugation (PC) [15] or time reversal (TR) [16]–[18], one also performs a relatively small set of measurements. The measured signals are time reversed (time-domain measurements) or phase conjugated (frequency-domain measurements) and reradiated into the domain of interest, and the original source current may be reconstituted

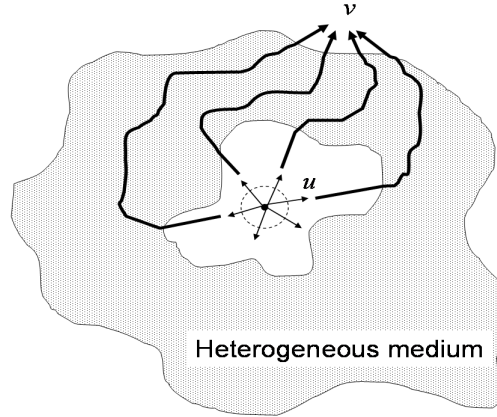


Fig. 1. A source emits radiation u into a homogeneous medium, and then the radiation propagates through a surrounding heterogeneous medium. The observed data v outside or within the heterogeneity corresponds to a superposition of the radiation emitted at different angles through a fictitious cylinder (dashed) surrounding the source. If the heterogeneities correspond to a draw from a random process, then the superposition (matrix) may also be viewed as a draw from a random process.

approximately. The resolution with which this refocusing occurs is dictated by the complexity of the propagation medium: the more complex the medium, the tighter the focus. It has been demonstrated that this may be viewed in the context of a “superresolution” phenomenon [19], whereby the complex propagation medium yields an effective aperture that is much larger than that of the original “small” physical aperture. This implies that the relatively small set of PC/TR measurements contains significant information about the source, and that the amount of information retained is enhanced as the propagation medium becomes more complex. Similar exploitation of propagation complexity and multi-path has also been used in the context of the related field of communications, for example in BLAST [20].

In this paper we demonstrate that the information content associated with such PC or TR measurements may be viewed from a CS perspective. Specifically, consider a line source radiating into a medium surrounded by heterogeneities (we consider the two-dimensional case to simplify the discussion). The source emits waves propagating in all directions out of a fictitious cylinder centered at the source (see Figure 1). In the presence of a complex medium, these different rays, emitted at different directions, may propagate through the complex media and arrive at the same physical location. Thus, a measurement taken at any point, due to a source in a complex

propagation medium, may be viewed as a linear combination of the waves emitted at different directions from the source. If the fields emitted from the aforementioned fictitious cylinder are a piecewise smooth function of angle φ , then they should be compressible in a wavelet basis (for example). Consequently, a linear combination of these emitted fields (linear combination of fields emitted at different sets of angles φ) may in principle constitute one CS measurement. Multiple measurements may therefore be viewed in terms of the CS measurement vector v ; the matrix relationship mapping $u \rightarrow v$ is constituted by the medium itself (via the Green's function of the propagation medium).

Using the measured v , and based on the CS theory summarized above, one should be able to use v to infer the radiated fields emitted from the source at all angles φ – or at least over the subset of emitted angles for which there is interaction with the complex media and subsequent propagation to the point of measurement. We refer to this as *in situ* compressive sensing, since the medium itself is being used to constitute the CS phenomenon; in this sense the medium and sensor are integrated into a CS whole. The connection between the propagation medium and the basis in which u is sparsely rendered is quantified below in terms of a mutual-coherence factor, recently introduced to CS by Candès and Romberg [21]. The mutual-coherence factor plays an important role in defining the number of required *in situ* CS measurements, based on the background propagation medium and the basis in which u is compressible. We demonstrate that when u is compressible in terms of a basis with extended spatial support (*e.g.*, a discrete cosine transform) the *in situ* CS measurements may even be effectively performed by exploiting wave propagation in vacuum. The impact of the background propagation medium on the complexity of the CS measurements is examined from multiple perspectives.

The remainder of the paper is organized as follows. In Sec. II we provide a concise summary of CS theory, setting the stage for understanding *in situ* CS. A detailed and fairly general description of *in situ* CS is provided in Sec. III, followed by a discussion of its properties in Sec. IV. A simple example is considered in Sec. V; this example has practical utility, but is sufficiently simple to provide relatively direct access to the characteristics of *in situ* CS. It is demonstrated that the appropriate background medium is connected to the basis in which the signal is sparsely represented, and that the complexity of the background medium also impacts the complexity of

the *in situ* CS measurement configuration. Conclusions and future directions are discussed in Sec. VI.

II. REVIEW OF COMPRESSIVE-SENSING THEORY

The field of compressive sensing was started by Candès, Romberg and Tao [6] by considering signals that are sparse in the Fourier domain, with this generalized subsequently by Candès and Tao [22] to signals that are sparse in general bases or frames. Donoho [7] considered further results along these lines, also (favorably) comparing compressive sensing to adaptive sensing techniques. As discussed further below, the work in [7], [22] deals with projecting the signal of interest onto random vectors. However, as discussed recently by Candès and Romberg [21], in many practical measurement systems truly random projections are difficult to implement, and they consequently introduce the idea of performing projections of the signal of interest onto an orthonormal basis (one different, in general, from the basis in which the signal is sparse). Results from [21] will play an important role in interpreting the *in situ* CS concepts introduced in this paper. In fact, the *in situ* CS framework developed here constitutes an example measurement system for which truly random projections are not feasible, and for which the theory in [21] was developed. As discussed further below, the *in situ* CS measurements performed in vacuum correspond to Fourier-like projections, directly relevant for the theory in [21], while for a more-complicated propagation media the projections are more sophisticated and do not explicitly correspond to orthogonal projections (but they are close).

In the wave problem of interest here, we will be considering complex signals u . The first paper in this field [6] considered complex signals, while [21] considered real signals and possibly complex projections. Other papers in this field [7], [22] have focused exclusively on real signals. However, it is noted in [22] that the theory extends directly to complex signals, except for negligible changes to some of the constants in the performance analyses. Consequently, in the discussion that follows we consider compressive sensing in the context of complex signals u , since the wave fields of interest for *in situ* CS are typically complex.

A. Sparsity

In the discussion below we adopt notation introduced by Donoho [7]. Consider a class U of m -dimensional complex signals. An information operator I_n maps any member of U to an n -dimensional complex vector, $I_n : U \rightarrow \mathbf{C}^n$. The information operator is of the form

$$I_n(u) = (\langle \xi_1, u \rangle, \dots, \langle \xi_n, u \rangle) \quad (1)$$

where $\langle \xi_i, u \rangle$ is an inner product and ξ_i are sampling vectors ($\langle \xi_i, u \rangle = \xi_i^H u$, where superscript H represents the complex transpose). We let A_n represent an algorithm that operates on the n -dimensional signal measured by the information operator I_n , and A_n attempts to reconstruct u , $A_n : \mathbf{C}^n \rightarrow \mathbf{C}^m$; the characteristics of such an algorithm are discussed below.

If the m -dimensional signals in U have special properties, u may be recovered accurately even when the number of measurements $n \ll m$, this yielding the terminology ‘‘compressive sensing’’. The exploitation of known constraints on the properties of signals in U may be viewed as a regularization of the mapping $A_n : \mathbf{C}^n \rightarrow \mathbf{C}^m$. In compressive sensing (CS) one exploits the fact that most natural signals u are compressible in an appropriate orthonormal basis, for example a wavelet [1], [2] or local Fourier [2] basis. The goal of CS is to directly measure the informative part of the signal u , such that the total number of samples that must be measured may be reduced substantially, potentially simplifying the hardware properties of the sensor digitization system. In this context the measurements are themselves directly performed in a compressive mode.

Focusing now on sparsity, let $\{\psi_i\}_{i=1,m}$ represent an orthonormal basis for m -dimensional signals, and therefore for $u \in U$ we have $u = \sum_{i=1}^m \theta_i \psi_i$, with $\theta_i \equiv \langle u, \psi_i \rangle$. The set U is termed compressible if for all $u \in U$

$$\|\theta\|_p \equiv \left(\sum_i |\theta_i|^p \right)^{1/p} \leq R \quad (2)$$

for some $0 < p < 2$ and for some $R > 0$. The case $p = 1$ corresponds to the well-known sparseness promotion employed within a Laplacian [11] distribution in Bayesian analysis, or ℓ_1 regularization [6], [7] resulting from an associated maximum *a posteriori* analysis [11]. As p

gets smaller the signals must be more sparse to satisfy (2) for a given R .

B. Random construction of information operator I_n

The signal u may be expressed as a column vector $u = \Psi\theta$, where θ is a column vector composed of coefficients $\{\theta_i\}_{i=1,m}$ and Ψ is an $m \times m$ matrix, the i th column of which is defined by the basis vector ψ_i ; the vector u is assumed sparse in the basis Ψ . The CS measurements may be represented by the n -dimensional column vector v , with $v = \Phi\Psi^H u$. The matrix resulting from the product $\Phi\Psi^H$ is responsible for the n projections; Φ is an $n \times m$ matrix, and the CS measurements may now be expressed as $v = \Phi\theta$.

A remarkable result proven by Candès and Tao [22] and Donoho [7] is that if the columns of matrix Φ are generated iid from an underlying distribution (*e.g.*, Gaussian or Bernoulli) then the process of measuring v and then recovering u is essentially optimal. Specifically, with “overwhelming probability”, when constituting the projection vectors $\{\xi_i\}_{i=1,n}$ (rows of Φ) in such a random manner, one may recover the underlying signal u . This optimality is manifested in the following sense [22]: By using randomly constituted projection vectors, one requires a near-minimal number of measurements n to recover the underlying signal u .

In practice the underlying signal u is recovered as the solution to the convex ℓ_1 regularized inversion

$$\min_g \|\theta(g)\|_{\ell_1} \quad \text{subject to} \quad \Phi\theta(g) = v = \Phi\theta(u) \quad (3)$$

There have been several algorithms developed to implement this inversion in practice [8], [10], [23]–[25]. In this paper we will be dealing with general complex data, which is different from most previous CS studies, for which real data have been primarily considered; in the Appendix we discuss how we have adapted CS to complex data, for performing the estimation of θ (and hence u) from the measured v .

C. Sparsity and incoherence

While randomly constituted projection vectors $\{\xi_i\}_{i=1,n}$ are optimal in the sense elucidated above, they have problems when considering practical implementations. For example, many physical sensing systems cannot easily implement such projections (the *in situ* CS framework presented here is one such physical CS system). This has motivated new work by Candès and Romberg [21]. Specifically, for the m -dimensional sparse signal of interest θ they consider an orthogonal basis B , with $B^H B = mI$, where I is the $m \times m$ identity matrix (Candès and Romberg [21] chose not to consider a normalized basis for reasons that become apparent below). The basis B may be represented as $B = \Upsilon\Psi$ for orthogonal matrix Υ and with Ψ representing the same sparseness basis as above; the $m \times 1$ complex measurement vector y is constituted as

$$y = B\theta = \Upsilon\Psi\theta = \Upsilon u \quad (4)$$

which is of the same form as for the random projections considered above, but we use the distinct B to underscore that above Φ was constituted via draws from an underlying random variable, while B is the product of two bases (Υ and Ψ); B is also a square $m \times m$ matrix, where Φ is an $n \times m$ matrix, with $n \ll m$.

Candès and Romberg [21] have demonstrated that if one *randomly* selects to measure n elements from the vector y , this now constituting the $n \times 1$ compressive-sensing measurement v , and n is sufficiently large, with overwhelming probability one may recover the underlying signal u using the same class of inversion algorithms as in (3). Importantly, a proportionality constant on the required n is

$$\mu(B) = \max_{i,k} |B_{ik}| \quad (5)$$

As discussed by Candès and Romberg, the form of $\mu(B)$ has very important implications for the desired choice of the basis Υ . Specifically, to minimize $\mu(B)$, and hence minimize the number of compressive sensing measurements n , the measurement vectors (rows of Υ) must be “spread out” in the Ψ domain [21]. For this reason $\mu(B)$ is often referred to as the *mutual coherence* and the goal is to design Υ such that $\mu(B)$ is $O(1)$. This property will play a very important

role in interpreting the *in situ* CS formulation to follow.

III. ANALYSIS OF *In Situ* COMPRESSED SENSING

A. Source excitation in homogeneous medium

To simplify the following discussion, we consider a two-dimensional scalar wave problem. The basic formalism extends naturally to more complex situations (vector problems in three dimensions), albeit with more cumbersome notation. The discussion below involves a level of wave analysis that is well known to experts (and non-experts) in that field, but the details are reviewed to introduce notation and to allow access to a broader audience.

Consider the field $u(x, z)$ excited by a time-harmonic source current $J_s(x, z)$ radiating into a homogeneous-medium, with corresponding wave equation

$$\left[\frac{\partial^2}{\partial x^2} + \frac{\partial^2}{\partial z^2} + k_o^2\right]u(x, z) = J_s(x, z) \quad (6)$$

where the wave speed in the medium is c , $k_o = \omega/c$, and the source is assumed time-harmonic with angular frequency ω (all field and current components are complex, and an $\exp(j\omega t)$ time dependence is suppressed throughout, with $j = \sqrt{-1}$). For electromagnetic problems, factors such as the frequency and permeability [26] are absorbed within the current $J_s(x, z)$.

Note that we are reusing notation from Sec. II. Specifically, in Sec. II u was the original signal of interest and v was a vector of the associated CS measurements. The reuse of this notation is done intentionally. In the discussion that follows the signal u , corresponding to a source radiating into a homogeneous medium, will be the signal of interest. We will subsequently introduce a second radiated signal v , corresponding to the same source, but now radiating into a background medium.

The Green's function for this two-dimensional homogeneous-medium problem satisfies

$$\left[\frac{\partial^2}{\partial x^2} + \frac{\partial^2}{\partial z^2} + k_o^2\right]u_G(x - x', z - z') = \delta(x - x', z - z') \quad (7)$$

where $\delta(x, z)$ is a two-dimensional delta function (line source). The fields radiated by the source $J_s(x, z)$ may be expressed as

$$u(x, z) = \iint dx' dz' J_s(x', z') u_G(x - x', z - z') \quad (8)$$

The two-dimensional homogeneous-medium Green's function is represented by the Hankel function $u_G(x - x', z - z') = \frac{j}{4} H_0^{(2)}[k_o \sqrt{(x - x')^2 + (z - z')^2}]$. We may employ the large-argument approximation to the Hankel function when $\sqrt{(x - x')^2 + (z - z')^2} \gg \lambda$, yielding

$$u(x, z) \approx \frac{1}{\sqrt{j8\pi k_o}} \iint \frac{dx' dz' J_s(x', z')}{[(x - x')^2 + (z - z')^2]^{1/4}} \exp[-jk_o \sqrt{(x - x')^2 + (z - z')^2}] \quad (9)$$

When the observation point (x, z) is distant relative to the spatial extent of the source (*i.e.*, in the far zone [26] of the source) we further have

$$u(x, z) \approx \frac{\exp(-j\pi/4)}{4\pi} \sqrt{\lambda/\rho} \iint dx' dz' J_s(x', z') \exp[-jk_o \sqrt{(x - x')^2 + (z - z')^2}] \quad (10)$$

where $\rho = \sqrt{x^2 + z^2}$. Under these conditions $\sqrt{(x - x')^2 + (z - z')^2} \approx \rho - x' \cos\varphi - z' \sin\varphi$, with $\cos\varphi = x/\rho$ and $\sin\varphi = z/\rho$, from which

$$u(\rho, \varphi) \approx \frac{\exp(-jk_o\rho - j\pi/4)}{4\pi} \sqrt{\lambda/\rho} \hat{J}_s(k_o \cos\varphi, k_o \sin\varphi) \quad (11)$$

where $\hat{J}_s(k_o \cos\varphi, k_o \sin\varphi)$ is the two-dimensional Fourier transform of the source currents, evaluated at spectral components $k_x = k_o \cos\varphi$ and $k_z = k_o \sin\varphi$.

Consider an arbitrary receiver array in the far zone of the excitation source J_s (see Figure 2). From (11) we observe that the information about $J_s(x, z)$ in the measured $u(x, z)$ is represented in the form of a scaled version of the Fourier transform of the currents, $\hat{J}_s(k_o \cos\varphi, k_o \sin\varphi)$. The particular observed spectral components are dictated by the angular relationship of the receiver relative to the source φ , and the range of spectral components observed is dictated by the physical size of the array aperture (which dictates the range of angles φ).

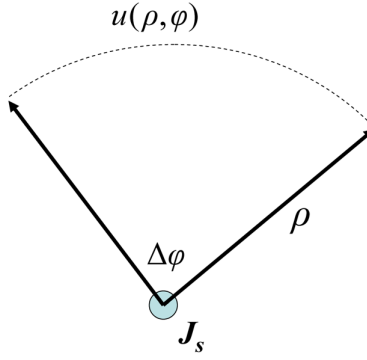


Fig. 2. The field $u(\rho, \varphi)$ radiated into a homogeneous medium from a source J_s , as viewed a distance ρ away, over an angular aperture φ .

The wave equation in (6) requires that the spectral content of the radiated fields satisfy $k_x^2 + k_z^2 = k_o^2$, but it is not required that both k_x and k_z be real. When $k_x > k_o$ the wavenumber k_z is imaginary, corresponding to evanescent fields in the z direction, and when $k_z > k_o$ the wavenumber k_x is imaginary, corresponding to evanescent fields in the x direction. Therefore, we note that in the far zone of the source, the observed radiated fields lose information about $J_s(x, z)$ contained in the evanescent fields.

B. Source excitation in heterogeneous medium

We now consider the same source $J_s(x, z)$ radiating into an inhomogeneous medium, with the latter defined by the spatially-dependent wavenumber $k(x, z)$. The heterogeneities characteristic of $k(x, z)$ are assumed to be of finite spatial extent (see Figure 3); let S_h represent the surface over which the material heterogeneity exists, *i.e.*, $k(x, z) \neq k_o$ for $(x, z) \in S_h$, and $k(x, z) = k_o$ otherwise. One may show that the fields radiated in such an environment satisfy [27]

$$v(x, z) = u(x, z) + \int \int dx' dz' u_G(x - x', z - z') [k^2(x', z') - k_o^2] v(x', z') \quad (12)$$

Because of the properties of $k(x, z)$ mentioned above, the double integral in (12) exists only over the finite support of S_h .

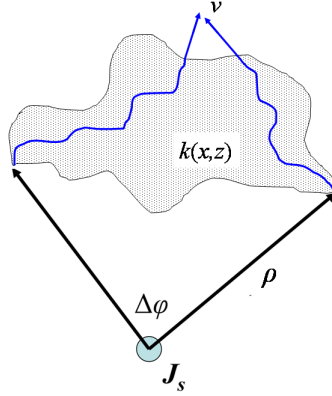


Fig. 3. The same source as considered in Figure 2, but now radiating into a finite heterogeneous medium. The scattered fields $v(x, z)$ at any point are a linear combination of the homogeneous-medium radiated fields that exist within the spatial extent of the heterogeneous medium.

The expression in (12) for $v(x, z)$ is valid for all (x, z) , and the traditional [25] solution methodology employs a finite set of basis functions with which to represent $v(x, z)$ for $(x, z) \in S_h$. We consider general subdomain basis functions [27], $\{p_i(x, z)\}_{i=1, M}$, and the union of the basis functions covers the support of S_h . The fields within the heterogeneous medium for $(x, z) \in S_h$ are therefore represented as

$$v(x, z) \approx \sum_{i=1}^M \alpha_i p_i(x, z), \quad (x, z) \in S_h \quad (13)$$

and for sufficiently large M (compact basis functions) the representation is accurate [27].

By imposing the condition in (12) at the center of each of the M basis functions (point matching [27]) we obtain

$$\alpha_l p_l(x_{cl}, z_{cl}) \approx u(x_{cl}, z_{cl}) + \int \int dx' dz' u_G(x_{cl} - x', z_{cl} - z') [k^2(x', z') - k_o^2] \sum_{i=1}^M \alpha_i p_i(x', z') \quad (14)$$

where (x_{cl}, z_{cl}) represents the center of the l th basis function, and an equation of the form in (14) is manifested for each (x_{cl}, z_{cl}) , $l = 1, 2, \dots, M$. This leads to a matrix equation for the unknown basis-function coefficients

$$u = Z\alpha \quad (15)$$

where α is a M -dimensional column vector representing the basis-function coefficients $\{\alpha_n\}_{n=1,M}$, and u is an M -dimensional column vector representing the source fields radiating into a homogeneous medium (considered in Sec. III-A), sampled at the center of the pulse basis functions. The $M \times M$ matrix Z has components as defined by (14).

From (15) it is clear that the basis-function coefficients α are a linear combination of the excitation fields u that reside within $(x, z) \in S_h$. For simplicity we assume that all of S_h resides within the far-zone of the source $J_s(x, z)$. For this case, using (11), the fields u are, apart from a known range-dependent scale factor, the Fourier transform of the source current. From (13), $v(x, z)$ for $(x, z) \in S_h$ is also a linear combination of the components in u , and hence of $\hat{J}_s(k_x, k_z)$. Finally, from (12) the fields $v(x, z)$ at any point (x, z) are a linear combination of $\hat{J}_s(k_o \cos \varphi, k_o \sin \varphi)$, over the range of angles φ consistent with the expanse of S_h relative to the source location (Figure 3).

Note that the angular extent of the rays measured in Figure 2 along a far-zone aperture, in free space, correspond to the same set of rays that sample the heterogeneous medium in Figure 3; these latter rays have the opportunity to be measured by the *in situ* CS measurement v . Hence, the information content with regard to u in these CS measurements has the potential to be consistent with the commensurate free-space measurement but, by exploiting the compressibility properties of $u(\rho, \varphi)$, there is the potential for fewer CS measurements v in Figure 3 than would typically be employed to sample the aperture in Figure 2. This is analogous to the superresolution property studied in time-reversal [28].

The principal result of this subsection may be summarized as follows. For a finite source $J_s(x, z)$ radiating into a finite heterogeneous medium situated in the far zone of the source, the radiated fields at any point satisfy

$$v(x, z) = \sigma_{x,z}^T \hat{J}_s \quad (16)$$

The m -dimensional column vector \hat{J}_s represents the unknown Fourier transform of the current $\hat{J}_s(k_o \cos \varphi, k_o \sin \varphi)$, sampled at m discrete angles φ consistent with the extent of the heterogeneity S_h . The column vector $\sigma_{x,z}$ is linked to observation position (x, z) , and it captures the properties of the heterogeneity, the homogeneous-medium Green's function, and it absorbs the range-dependent scale factors $(\exp(-jk_o \rho - j\pi/4) \sqrt{\lambda/16\pi^2 \rho})$ associated with $u(x, z)$. The specific and simple example considered in Sec. V will make these observations more concrete.

If n measurements are performed at multiple positions (x, z) in the presence of the heterogeneous medium, the set of measurements v are expressed in matrix form as

$$v = \Sigma \hat{J}_s \quad (17)$$

where here v is a n -dimensional column vector, \hat{J}_s is the m -dimensional column vector defined above, and Σ is a $n \times m$ matrix defined by the properties of $k(x, z)$ and the Green's function $u_G(x, z)$.

To make the above analysis more suggestive, we may express the vector \hat{J}_s in the form of an inverse orthonormal transform $\hat{J}_s = \Psi \theta$, where Ψ is a matrix as in Sec. II representing the wavelet basis (or other compressive basis for \hat{J}_s), and θ represents the associated basis-function coefficients. Similarly, we define $\Phi = \Sigma \Psi$, from which $v = \Phi \theta$.

From the CS theory (Sec. II), if \hat{J}_s is compressible in the orthonormal basis Ψ , and if the matrix $\Phi = \Sigma \Psi$ satisfies the properties of a CS matrix (discussed further in Sec. IV), then it should be possible to reconstruct \hat{J}_s accurately with a relatively small number of measurements performed in the presence of a heterogeneous medium (these measurements defining v).

The spectral current $\hat{J}_s(k_o \cos \varphi, k_o \sin \varphi)$ is typically a smooth function of angle φ for source distributions of interest, and therefore most of the m coefficients θ_i in a wavelet transform (for example) of \hat{J}_s will be small. Consequently, based on CS theory, it is anticipated that a relatively small number of CS measurements v will be required to recover $\hat{J}_s(k_o \cos \varphi, k_o \sin \varphi)$ accurately over the angular extent afforded by S_h .

C. Implications

From the above discussion we note that \hat{J}_s (and hence the far-zone radiated fields) may be estimated by performing a relatively small number of measurements in the presence of a medium defined by a finite heterogeneous region S_h . Therefore, anything that may be recovered using $u(x, z)$ as measured on the associated far-zone extended antenna aperture (Figure 2) should also be recoverable from the relatively small number of CS measurements v . For example, the quality with which one may reconstruct $J_s(x, z)$ based on measurements v should be at least as good as that corresponding to measurements in a homogeneous medium in the far zone, using a commensurately sized antenna aperture.

This motivates the following possible application. Assume we are interested in measuring the fields emitted by $J_s(x, z)$ over a large angular extent, as radiated into a homogeneous medium (*e.g.*, antenna characterization). A traditional approach would perform these measurements in air with a large number of spatial sampling points. The CS alternative to acquiring the same information would place the same source $J_s(x, z)$ in the presence of a known inhomogeneous medium, with spatial extent S_h commensurate with the desired range of far-zone angles. A relatively small number of CS measurements are performed, consistent with the compressibility of the angle-dependent radiated fields, and CS inversion is then performed to determine the associated far-zone radiated fields over the desired range of angles. A simplified form of such an experiment is examined in Sec. V. In addition, as discussed in Section IV, the required number of *in situ* CS measurements is dictated by the mutual coherence [21] between the medium Green's function and the basis Ψ in which u is sparsely rendered. It is demonstrated that when u is sparsely represented with an extended basis like the DCT, the *in situ* CS may be constituted in terms of a relatively small number of measurements *performed in vacuum*.

IV. PROPERTIES OF *In Situ* CS PROJECTIONS

From (16), the *in situ* CS measurement at point (x, z) corresponds to a projection $v(x, z) = \sigma_{x,z}^T \hat{J}_s$, where \hat{J}_s represents the source current in the spectral domain. An alternative way of obtaining this expression is by considering the current in the space-domain $J_s(x', z')$, and

integrating $J_s(x', z')$ with the appropriate Green's function [26] $g(x, z; x', z')$ to yield the radiated fields $v(x, z)$ at the point (x, z) :

$$v(x, z) = \int dx' dz' g(x, z; x', z') J_s(x', z') = \int dx' dz' g_w(x, z; x', z') J_s(x', z') \quad (18)$$

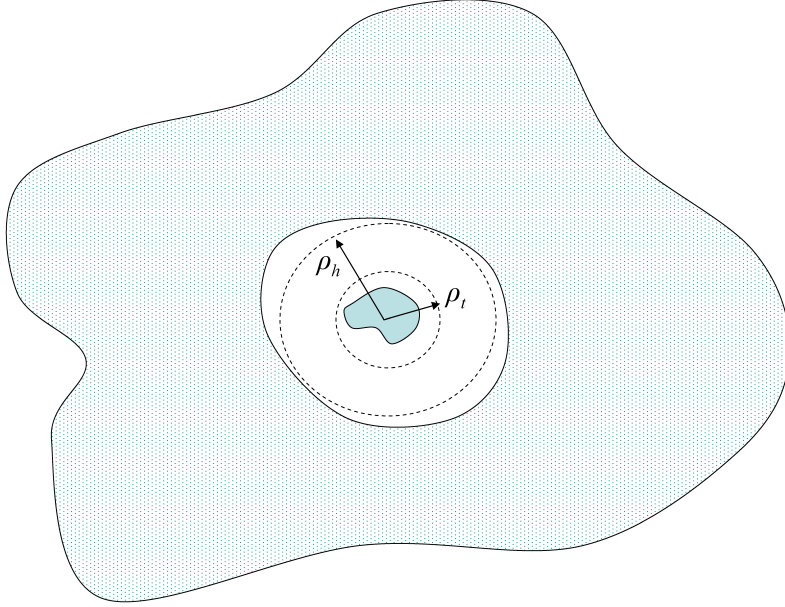


Fig. 4. A general current distribution (in center) is surrounded immediately by vacuum, with a heterogeneous medium surrounding this vacuum. A window function is applied to the Green's function, before converting into the spectral domain. In the region with radii less than ρ_t the window has an amplitude of one, and outside this region the window tapers down to zero, before reaching the surrounding medium, at a radius ρ_h .

Note that in the discussion in Sec. III u_G was used to represent the *free space* Green's function, where now we employ $g(x, z; x', z')$ to represent the Green's function for a general background environment (free-space being a special case). In addition, in (18) we introduce a windowed Green's function $g_w(x, z; x', z')$, where the window function has unit amplitude over the support of the current $J_s(x', z')$, and it tapers to zero away from the current (when present); see Figure 4. Using Parseval's theorem, (18) may be expressed in the spectral domain as

$$v(x, z) = \frac{k_o}{4\pi^2} \int_0^{2\pi} d\varphi \hat{J}_s(\varphi) \hat{g}_w(x, z; \varphi + \pi) \quad (19)$$

where the one-dimensional angular integral is manifested because only propagating waves [29] are observed, at frequency ω , and the spectral angle φ is related to the two-dimensional spectral variables (k_x, k_z) via $k_x = k_o \cos\varphi$ and $k_z = k_o \sin\varphi$, where we recall $k_o = \omega/c$ where c is the speed of light in vacuum.

Now returning to (16), it is observed that $\sigma_{x,z}$ is a vector representing $\frac{k_o \Delta\varphi}{4\pi^2} \hat{g}_w(x, z; \varphi + \pi)$ sampled in increments $\Delta\varphi$ with respect to φ , over the support $\varphi \in [0, 2\pi)$. Each row of the matrix Σ in (17) corresponds to the sampled spectral Green's function $\frac{k_o \Delta\varphi}{4\pi^2} \hat{g}_w(x, z; \varphi + \pi)$ for a distinct observation point (x, z) , corresponding to the associated measurement $v(x, z)$. We now consider the matrix product $P = \Sigma^H \Sigma$, the ik th element of which approximately (within the approximation of the sampling in φ) satisfies the proportionality relationship

$$P_{ik} \propto \int dx \int dz g_w(x, z; x'_i, z'_i) g_w^*(x, z; x'_k, z'_k) \quad (20)$$

where Parseval's theorem has been used again. One may recognize the term to the right in (20) as the time-reversal operator [17], [28]. Specifically, a source at (x'_k, z'_k) emits fields that are observed at the arbitrary point (x, z) ; the complex conjugation of $g_w(x, z; x'_k, z'_k)$ in (20) is analogous to time-reversal (although here we only consider a single frequency) of the fields observed at (x, z) . The phase conjugated fields at a point (x, z) are then propagated to the point (x'_i, z'_i) , through multiplication with Green's function $g_w(x, z; x'_i, z'_i)$. The double integral in (20) corresponds to superposing the phase-conjugated fields from all points (x, z) – therefore the phase-conjugated receiver/transmitters exists over all (x, z) within the window circumscribing the source.

We now consider the same current $J_s(x', z')$ radiating into two different types of media (see Figure 6). In one case the current radiates into a vacuum (free-space) medium, and in the other the current radiates into the heterogeneous medium of the type discussed in Section III. The receiver points are oriented in both cases in a circle around the domain, sampled at the Nyquist rate. In both of these distinct scenarios the fields observed at a given point around the circle

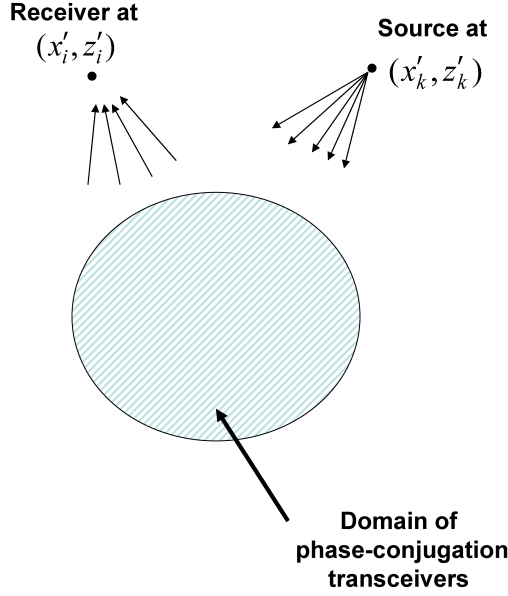


Fig. 5. Depiction of phase-conjugation phenomenon, associated with a source at (x'_k, z'_k) , with the phase conjugation transceivers located in the domain characteristic of the source current J_s . The fields radiated by the transceivers are observed at (x, z) . For (x'_k, z'_k) and (x'_i, z'_i) separated by more than a half wavelength, it is anticipated that the fields observed at (x'_i, z'_i) will be very weak, implying P_{ik} in (20) will be very small for this case, while peaking for $(x'_k, z'_k) \rightarrow (x'_i, z'_i)$.

correspond to a particular measurement $y(x, z)$. For the case of a surrounding vacuum, the measurements are represented as $y_{vac}(x, z)$, and for the heterogeneous surrounding medium as $y_{het}(x, z)$. The vector of all such measurements, at all receiver points around the circle (Figure 6) are denoted y_{vac} and y_{het} and expressed

$$y_{vac} = \Sigma_{vac} \Psi \theta \quad y_{het} = \Sigma_{het} \Psi \theta \quad (21)$$

where Σ_{vac} and Σ_{het} represent the matrix Σ in (17) for the respective background medium. Because of the aforementioned properties of $\Sigma^H \Sigma$ (equation (20)), the matrix products $\Sigma_{vac}^H \Sigma_{vac}$ and $\Sigma_{het}^H \Sigma_{het}$ are strongly diagonal-dominant. Moreover, because of symmetry in a surrounding vacuum medium, $\Sigma_{vac}^H \Sigma_{vac}$ will have constant values down the diagonal, and along adjacent diagonals. If the background heterogeneities are relatively uniformly distributed azimuthally around the current source, the same properties will be approximately true for $\Sigma_{het}^H \Sigma_{het}$.

While this is not exactly the same situation as considered by Candès and Romberg [21] and summarized in Sec. II-C, it is very much of the same form; specifically, in Sec. II-C the projection matrix Υ was exactly orthogonal ($\Upsilon^H \Upsilon = mI$), where here $\Sigma^H \Sigma$ is nearly diagonal, as a result of the properties discussed with respect to P_{ik} in (20). Based on [21], one would anticipate that it should be possible to randomly sample components of y_{vac} or y_{het} from about the circle in Figure 6 (these random samples constituting CS measurements v_{vac} and v_{het}), and that with sufficient such measurements the CS inversion framework may be employed to estimate θ and hence u . However, key to determining the required number of such measurements n is the mutual coherence [21], represented in Sec. II-C as $\mu(B) = \max_{i,k} |B_{ik}|$; here B is replaced with either $\Sigma_{vac} \Psi$ or $\Sigma_{het} \Psi$, respectively for vacuum and heterogeneous medium. Importantly, the mutual coherence will depend on the properties of the background environment, dictating the matrix Σ , and on the basis Ψ selected for sparse representation of u . These issues are considered in detail in Section V.

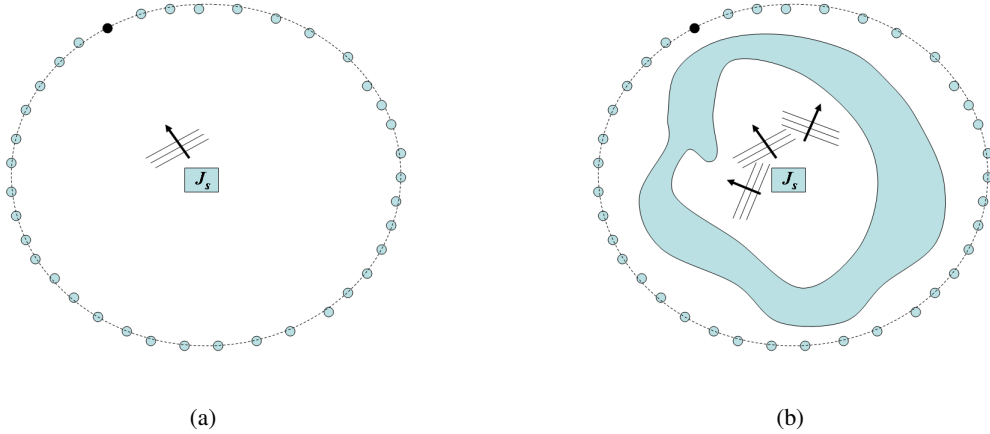


Fig. 6. Current source J_s situated in the center of a circular array of receivers. In (a) the system resides in vacuum, while in (b) there is a heterogeneous medium surrounding the current source. Depicted are the wavefronts (spectral components) notionally observed at a particular receiver (denoted in black). In (a) one dominant spectral component contributes, while in (b) multiple components contribute to the field observed at the receiver, as a consequence of multipath

The above discussion relied importantly on linkages to time-reversal [17] or phase conjugation. Specifically, the approximate orthogonality of the *in situ* CS projections in (20) has made direct use of characteristics of time reversal (or phase conjugation). To further make linkages to the work of Candès and Romberg, the dimensionality of the matrix Σ should be consistent with the

number of unknowns in the sparse vector θ . In Figure 6(a) the sensors are distributed around a circle to realize a sufficient number of possible measurements and to assure via (20) that Σ is strongly diagonal dominant. Note that in Figure 6(a), corresponding to the free-space (vacuum) case, multiple sensors at the same angle (but different radii) will *not* have Green's functions that are approximately orthogonal; considering Figure 5, for a source at (x'_k, z'_k) in free space (vacuum), the phase conjugation within the shaded circle (window) will produce a narrow *beam* propagating back to (x'_k, z'_k) , and therefore approximate orthogonality is *not* manifested if other sources are aligned at the same angle. Therefore, in the case of a vacuum medium, the distribution of the sensors around a circle (or circumference) is a requirement. This requirement may not be necessary for a complicated surrounding medium as in Figure 6(b), underscoring the potential advantage of the latter. Specifically, as depicted in Figure 7, if the surrounding medium manifests complicated wave propagation, the approximate orthogonality reflected in (20) may be manifested even for sensors at the same angle relative to the center of the imaging domain, due to the superresolution constituted by time-reversal [17], [28]. Hence, the sensors may be situated more conveniently, in relative close proximity of one another, rather than being distributed around a circle.

Summarizing, in the context of *in situ* CS, the properties of the background medium are manifested from two perspectives. First, the details of the background medium impact the mutual coherence, and therefore dictate the number of required CS measurements. In addition, the complexity of the surrounding medium will impact the positions at which sensors may be placed, with a more-compact sensor arrangement manifested as the propagation medium becomes more complicated. However, the utility of the more-compact arrangement of sensors is mitigated by the required complicated propagation environment, and also the requirement that the associated Green's function must be known accurately (of course, by contrast, the free-space Green's function is known exactly).

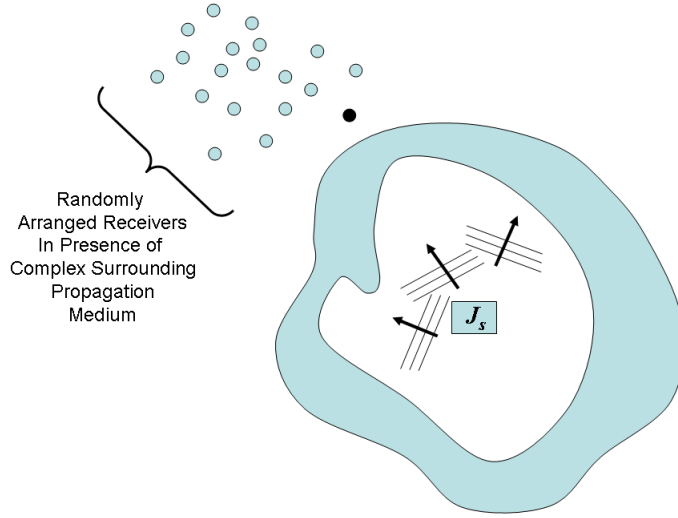


Fig. 7. Potential distribution of *in situ* CS sensors when the source is surrounded by a complex propagation medium.

V. ILLUSTRATIVE EXAMPLE

A. Problem description

To demonstrate the concepts introduced above, we consider a two-dimensional current $J_s(x, z)$ situated in two distinct environments: (i) in vacuum with the receivers situated around a circle of radius $200\lambda_c$, and (ii) the same source situated within two perfectly reflecting plates (Figure 8); λ_c represents the center wavelength of the wideband source. Using image theory, the fields at any point within the plates may be represented as a superposition of fields due to sources in free space, defined by the original source and an infinite set of image currents [26]. Specifically, the fields $v(x, z)$ at any point within the waveguide, at sufficient distance from the source, may be expressed as

$$v(x, z) = \frac{\sqrt{\lambda} \exp(-j\pi/4)}{4\pi} \sum_{n=-\infty}^{\infty} (-1)^n \exp(-jk_o \rho_n) \hat{J}_s(k_o \cos \varphi_n, k_o \sin \varphi_n) / \sqrt{\rho_n} \quad (22)$$

$\rho_n = \sqrt{(x - 2nd)^2 + z^2}$, $\cos \varphi_n = (x - 2nd) / \rho_n$, and $\sin \varphi_n = z / \rho_n$, where to simplify (22) the center of the source is assumed located at $(x = 0, z = 0)$ and the plates are at $x = \pm d$, although the source may readily be considered at any point within the waveguide. In the examples that

follow, the specific source current considered is the quadrupole reflected in Figure 9.

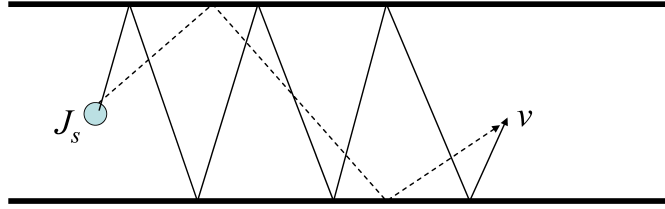


Fig. 8. Two-dimensional current J_s radiating in the presence of two parallel perfectly reflecting plates. Two (of many) ray paths to an example *in situ* CS measurement point are shown; multiple such measurements are performed to infer the angle- and frequency dependent properties of the source J_s radiating into a homogeneous medium.

For simplicity, the discussion in Section III assumed that the *in situ* CS measurements were performed to infer the angle-dependent radiated field at a single frequency. We now generalize this to the goal of inferring the angle- and frequency-dependent properties of the radiated fields. We may view this as using *in situ* CS to infer an image, where now one dimension of the image corresponds to discretized angles, and the other dimension corresponds to discretized frequencies; moreover, the image is complex.

We now discuss special properties of this problem that simplify the CS processing. Recall again that the *in situ* CS measurements may be expressed as $v = \Sigma \hat{J}_s$, where now \hat{J}_s is viewed as the aforementioned image (function of angle and frequency); here Σ is an $n \times m$ matrix, corresponding to the n randomly selected sensor positions. Assume that each CS measurement is taken at a single position in the waveguide and at a single frequency; consequently, each row of the matrix Σ is all zeros, except for the components corresponding to the frequency being measured.

The two-dimensional source current (as a function of angle and frequency) may be represented in a two-dimensional (*e.g.*, wavelet) basis as $\hat{J}_s = \Psi\theta$, where θ again represents the basis-function coefficients. The CS analysis is performed with the matrix equation $v = \Phi\theta$, where $\Phi = \Sigma\Psi$. The form of Σ simplifies the required computations substantially. Specifically, each two-dimensional coefficient may be interpreted as an inner product between the two-dimensional “image” \hat{J}_s and

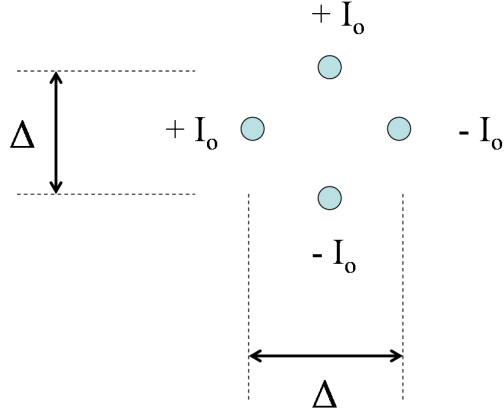


Fig. 9. Schematic of four current elements arranged to constitute a quadrupole source.

a tensor-product matrix, where the ij th example of the latter is represented as $\psi_i\psi_j^T$; ψ_i is a column vector representing the i th one-dimensional projection vector [2]. A given component of the matrix Φ is an inner product between a row of Σ and a column of Ψ , where the latter column is an appropriately "unwrapped" version of a tensor product of the form $\psi_i\psi_j^T$. Because of the special property of a row of Σ , for a single-frequency CS measurement, a given component of Φ may be represented as $c_k^T\psi_i)\psi_j(k)$ where c_k is the column in the image \hat{J}_s corresponding to the particular (here k th) frequency under test, and $\psi_j(k)$ is the k th component of the basis vector ψ_j .

The physical geometry of the problem is summarized in Figure 10. The true "images" characteristic of the spectral properties of this source are shown in Figure 11, represented as 256×256 images; one image is associated with the real part of the spectral current and the other is associated with the imaginary part.

B. Mutual coherence calculations

As discussed in Section II-C, the number of required CS measurements is proportional to the mutual coherence, based on the theory of Candès and Romberg [21]. We consider two relative extremes for the selection of Ψ : (i) the discrete cosine transform (DCT), and (ii) the Haar wavelet. Note that a free-space experiment as in Figure 6(a) essentially measures the spectral-

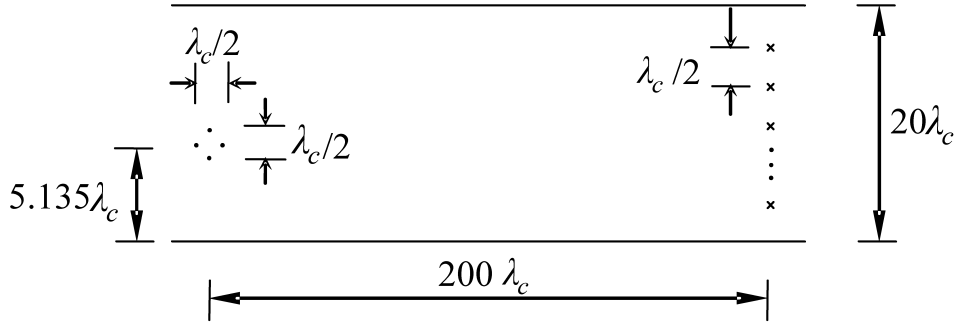


Fig. 10. Geometry of problem under test, with dimensions shown with respect to the center wavelength. A detailed depiction of the currents is shown in Figure 9, with the current $I_o = \exp(j\pi/6)$.

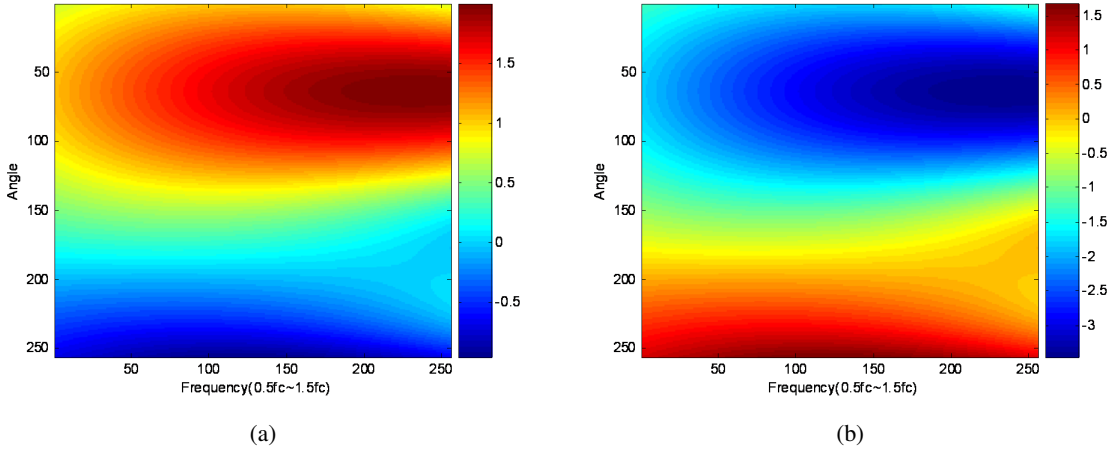


Fig. 11. Real and imaginary parts of the current source. The data are depicted as 256×256 images; the vertical axis spans from $\varphi = 0^\circ$ to $\varphi = 180^\circ$, from top to bottom, and the horizontal axis depicts frequency from 0.5 to 1.5 times the center frequency. (a) real part, (b) imaginary part.

domain current $\hat{J}_s(\varphi, \omega)$ at a *single* angle φ dictated by the position of the receiver relative to the current center (see (11)). This localization in the space of Σ is particularly well matched to the spread-out nature of the DCT basis, from the standpoint of mutual coherence. By contrast, the spectrally spread-out nature of Σ for the case of the waveguide (the infinite set of images yield multiple significant spectral components in the angle φ) is better matched to the localized wavelet basis (here the Haar, although other wavelets – for example, the Daubechies 4 and 8 – were found to give similar mutual-coherence values). The mutual coherence for the two choices of measurement geometries and for the two choices of Ψ are summarized in Table I.

The elements of Table I were computed as follows. Each *in situ* measurement, which corresponds to a row of the matrix Σ , is associated with one receiver location and one frequency. For the free-space measurements as in Figure 6(a), the receivers are situated uniformly around one-half of a circle, while for the waveguide the receivers are situated uniformly at one end of the waveguide (see Figure 10). The spectral Green’s functions for both geometries may be computed analytically. Following the ideas in [21], to compute the mutual coherence each row of Σ is normalized such that the diagonal of $\Sigma^H \Sigma$ has amplitude m , corresponding to the total number of possible measurements (from which the CS measurements are randomly selected). These normalized Green’s functions were then employed within the mutual-coherence calculations.

TABLE I
MUTUAL COHERENCE AS A FUNCTION OF BASIS Ψ AND MEASUREMENT ENVIRONMENT.

	DCT Basis	Haar Basis
Free Space	2.0	128.0
Waveguide	9.8	118.3

C. Reconstruction accuracy

Based on the numbers in Table I, one anticipates that when Ψ corresponds to the DCT basis the free-space *in situ* CS measurements will converge more quickly than the waveguide counterpart, while for the Haar basis the waveguide-based measurements are expected to converge more quickly. However, in addition to being proportional to the mutual coherence, the theory of Candès and Romberg [21] indicates that the number of measurements is also proportional to the number of significant coefficients in the basis weight vector θ . Because of the simple form of the current considered here, as indicated in Figure 11, one may show that θ is significantly more sparse in the DCT basis than it is in the Haar (to achieve 90% relative mean-square error, the DCT requires $S = 6$ nonzero coefficients, while a six-level Haar transform has $S = 30$). Based on this, we also anticipate that use of the the DCT basis will yield CS inversion results that converge significantly faster than based on the Haar basis.

In the *in situ* CS results we randomly select n receiver positions and associated frequencies,

and we present the fractional error as a function of n (for example, for the free-space case, we randomly select sensors situated about the circumference of a $200\lambda_c$ radius circle). Since the measurements are selected randomly, we present average results as well as error bars that reflect one-standard-deviation variation across the multiple runs (here 100 random runs for each case). The results in Figures 12 and 13 confirm expectations based on the mutual-coherence calculations and based on the sparseness of the underlying signal u in the DCT and Haar bases. Specifically, we note that the DCT-based relative errors converge more quickly than those based on the Haar wavelet, because the underlying spectral current is significantly more compressed in the DCT than it is in the Haar basis. In addition, we note that for the DCT basis the free-space measurements converged slightly quicker than those in the waveguide, while this trend is reversed for the Haar basis; as indicated above, this behavior is anticipated by the mutual-coherence computations in Table I.

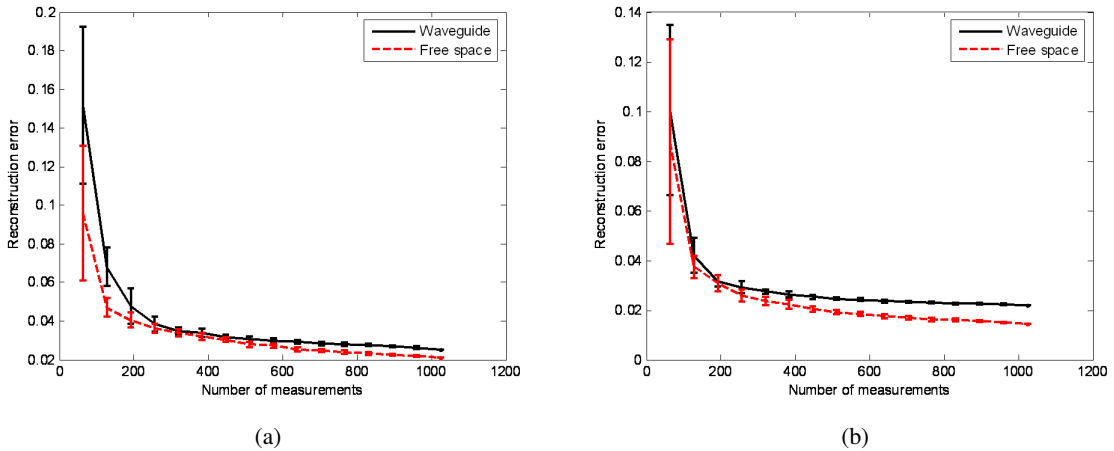


Fig. 12. Relative error of the *in situ* CS inversions for Ψ based on the DCT, for measurements performed in free space and within the waveguide. (a) real part, (b) imaginary part.

To provide a visual representation of the reconstruction accuracy of the *in situ* CS inversions, in Figure 14 we present an example reconstruction based on the DCT basis within the waveguide, using 64 measurements (although not shown here, if one performs 64 measurements in free space, *uniformly* sampled in angle-frequency space, and applies linear interpolation, the quality of the reconstructions are significantly worse than those produced by CS in Figure 14). It is observed, with comparison to Figure 11, that the CS reconstruction is highly accurate. A brief discussion

of how the CS inversion is implemented here, for complex data and complex projections, is provided in the Appendix.

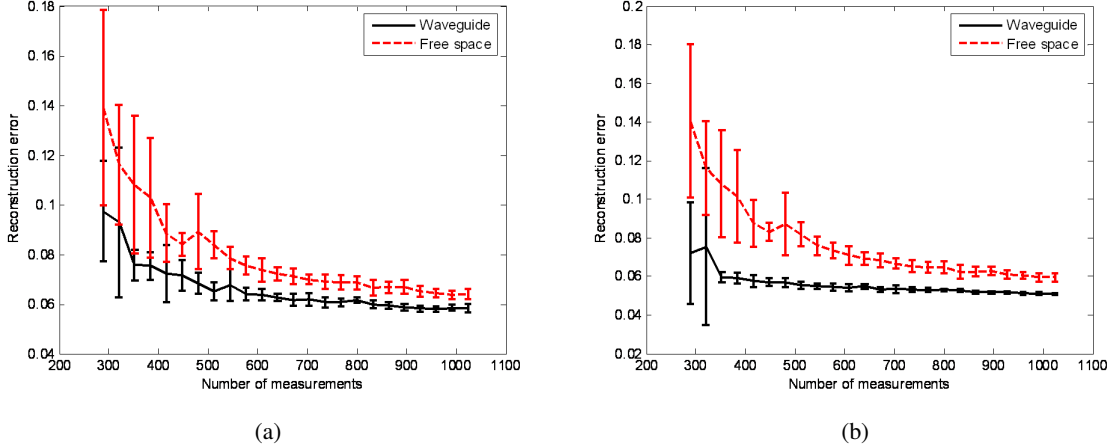


Fig. 13. Relative error of the *in situ* CS inversions for Ψ based on the Haar wavelet, for measurements performed in free space and within the waveguide. (a) real part, (b) imaginary part.

D. Discussion

For the reconstruction of the 256×256 complex “images” reflected in Figure 11, the *in situ* CS yields substantial reduction in the number of required number of angle-frequency measurements. When the spectral-domain current under test is sparse in the DCT basis, this analysis indicates that the random free-space measurements are slightly better than those within the waveguide, in the sense of the rate of convergence. This was the case for the simple quadrupole current considered here. However, real antenna sources are anticipated to often yield a more-sophisticated spectral-domain pattern than the quadrupole, and for these more-realistic cases it is anticipated that a wavelet-based basis Ψ may be more appropriate than the DCT. Based on the mutual-coherence analysis presented here, for such a more-sophisticated source the waveguide-based measurements are expected to potentially be more efficient.

As a second consideration, we note that measurements of the type in Figure 6(a) are often more difficult to perform than those performed within the waveguide (Figure 10). This is because measurements like those in Figure 6(a) must be performed at a large set of angles, corresponding to large variation of the relative source-receiver angle, and that importantly such

measurements must typically be performed within an anechoic chamber (such facilities are often expensive to construct). By contrast, the measurements in Figure 10 are performed within an *echo* chamber, rather than an anechoic chamber, and therefore such a measurement facility is relatively inexpensive to build. Moreover, based on the considerations associated with Figure 7, the physical range of required sensor positions is far more limited than those associated with Figure 6(a), since for the former the multiple angle directions are achieved by exploiting the multi-path of the medium.

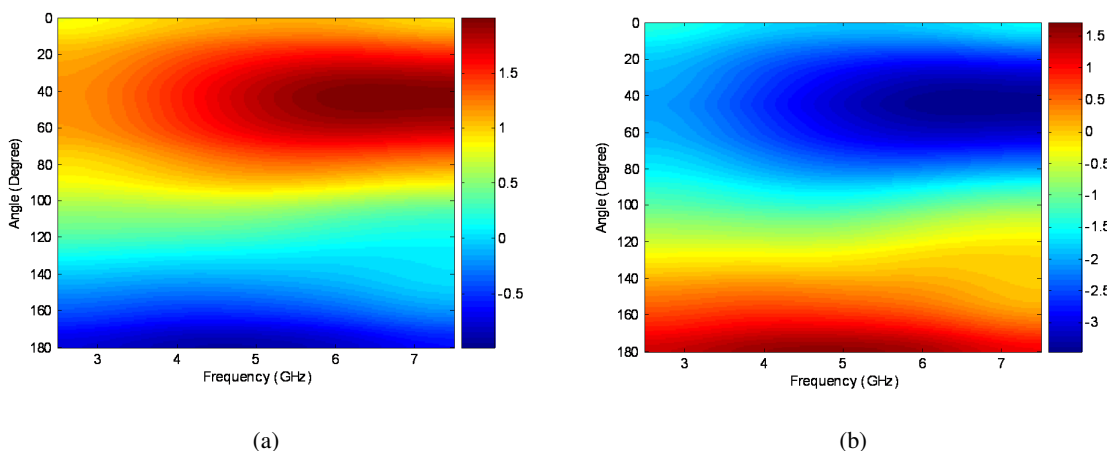


Fig. 14. *In situ* reconstruction based upon the DCT basis, with measurements performed within a waveguide (64 total measurements, across angle and frequency). (a) real part, (b) imaginary part.

Concerning the resolution of these experiments, note that within the waveguide the *physical* aperture of the receivers relative to the source center is only 5.8° (CS samples are selected at random points over this aperture), while for the free-space results the samples are selected randomly from a 180° aperture. From this standpoint, the accuracy of the waveguide-based *in situ* CS reconstructions in Figures 12 and 13 is remarkable. To achieve this “superresolution” within the waveguide, the *in situ* CS results have exploited the multi-path reflected in Figure 8, in the same sense considered previously in time-reversal studies [17], [28]. However, in previous time-reversal studies one was interested in localizing the source through refocusing, while here we infer the entire angle-frequency spectrum of the source. We note that the *in situ* CS framework, for a complicated propagation medium like the waveguide, also inherits from time-reversal the sensitivity of the inversion to use of the proper Green’s function in Σ . In our studies for the

waveguide problem, we have found that the quality of the CS inversion is very sensitive to using the proper Green's function, as discussed by [28] with regard to time reversal. However, there have recently been ideas from signal processing considered to reduce these sensitivities in the context of time reversal [18], and such concepts may be considered in future *in situ* CS studies. This is a significant advantage of the aforementioned free-space CS measurements, for which the Green's function is simple and known exactly.

While the waveguide-based measurements provide several important practical advantages, there are many anechoic measurement facilities that exist today around the world. Measurements performed within such facilities approximate experiments performed in vacuum. The analysis presented here indicates that one may use ideas from CS to significantly reduce the number of required measurements within these *existing* facilities. Finally, within the context of the *in situ* CS simulated measurements considered here, we randomly sampled the data in (21) in both sensor position and frequency (each measurement was a different randomly sampled frequency and sensor location). In a practical system it is often relatively simple to sweep across multiple frequencies, while the physical movement of the sensor is more complicated. Therefore, in practical *in situ* CS measurements of the type considered here, one will typically sample the spatial sensor positions randomly, and then measure *all* frequencies at these sampled spatial points; this is expected to reduce the total number of different spatial positions of the sensors one must consider.

E. Comparison to time-reversal

Recognizing the aforementioned properties of the matrix Σ employed within the *in situ* CS measurements, an associated time-reversal [17] result may be represented as

$$\Sigma^H v = \Sigma^H \Sigma \hat{J}_s; \quad (23)$$

this may be considered as an alternative to the (spectral angle)-frequency image considered in Sec. V-E. The expression $\Sigma^H \Sigma$ is the well-known time-reversal operator [28].

In Figure 15 are plotted the real and imaginary parts of $\Sigma^H v$. We observe that these images of

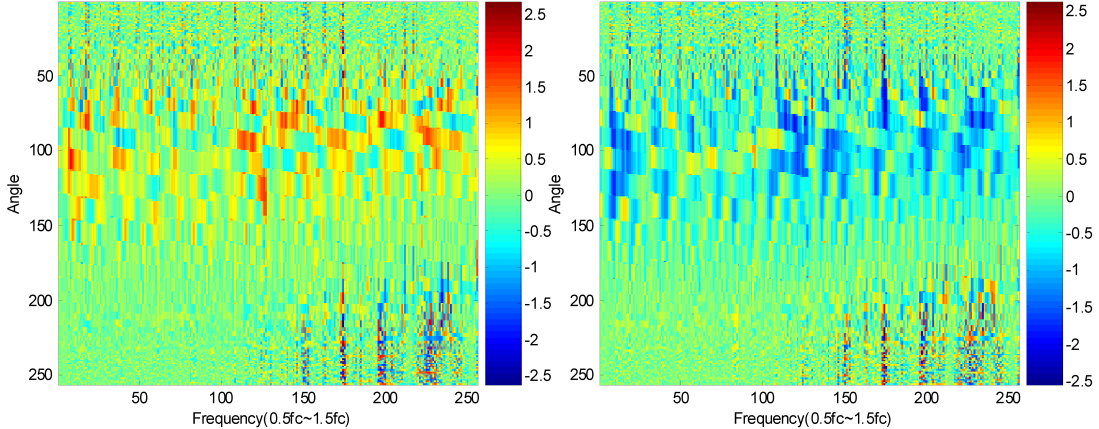


Fig. 15. The real (left) and imaginary (right) part of the vector constituted by $\Sigma^H v$, corresponding to a spectral analysis of the time-reversed signal.

the (spectral angle)-frequency plane capture some of the structure in the spectral properties of the source, but not nearly as effectively as the CS-based inversion considered in Sec. V-E. The results in Figure 15 correspond to the case of 1024 measurements.

VI. CONCLUSIONS

It has been demonstrated that the fields observed at a point in a general propagation medium may be viewed as a linear combination the fields from the same source, as radiated into a homogeneous environment. In the context of compressive sensing (CS), the former fields represent the data v and the latter u . Exploiting the compressible nature of most fields, as a function of position and frequency, one may use CS to infer u from v , with the number of required measurements for v small relative to those typically required for u . This has been referred to as *in situ* CS, because the propagation medium is itself exploited to perform the compressive measurements. The basic concept has been demonstrated for the problem of a source radiating in the presence of parallel plates and in vacuum, with encouraging results demonstrated. In addition to providing a relatively simple demonstration of the theory, the waveguide-based radiation measurements may be used to constitute a new framework for providing compressive antenna characterization. Rather than measuring an antenna pattern in the far zone and in free space as a function of angle, the antenna may be placed within two large plates (or other multi-path-generating medium) and

a relatively small number of measurements may be performed, with the angle and frequency dependent radiation pattern inferred using CS techniques like those considered here. However, particularly when the signal of interest is compressible in a basis like the DCT, one may employ CS techniques even for free-space measurements, with this of importance for accelerating the rate at which experiments are performed within existing anechoic chambers.

There are several areas of interest for future research. The example considered in Sec. V is a simplified version of a source emitting radiation in an *acoustic* channel, for example. In a practical example the (sea) bottom will typically not be a perfect reflector, and the sea depth will likely not be constant. It is of interest to examine the extension of the CS theory to the case of inferring the radiation spectra from an underwater passive source. This may involve a modification of the mathematical framework whereby one maps the observed compressive data v to the desired signal u . Specifically, one may wish to consider uncertainty in the matrix Σ , this matrix constituting the relationship $v = \Sigma\theta$, where θ represent the wavelet coefficients of u . The uncertainty in Σ will reflect uncertainty in the acoustic-channel properties.

In the example presented here we considered a simple quadrupole source, which is highly compressible in a DCT basis. Based on the mutual-coherence analysis, this situation is particularly well suited for CS measurements performed in vacuum, at multiple randomly selected angles. As the source radiation fields become more sophisticated, it is anticipated that localized (*e.g.*, wavelet) bases will become more relevant, and for such a basis the mutual coherence analysis indicates that a more-complex background medium is desirable for efficient *in situ* CS measurements. It is desirable in future work to examine more-realistic source currents (antennas), and ideally to do actual physical measurements to demonstrate the *in situ* CS concepts.

ACKNOWLEDGEMENTS

The authors thank the reviewers for very important technical suggestions, these significantly improving the quality of the revised text. The authors also gratefully acknowledge financial support from DARPA, under the Mathematical Time Reversal (MTR) program.

APPENDIX

We provide a very brief summary of how the CS reconstructions were performed here, for complex basis-function coefficients θ , in real basis Ψ , using complex projections defined by the matrix product $B = \Sigma\Psi$ (the matrix Σ is complex, manifested by the wave propagation discussed in Section III). A more-complete discussion of the method presented here will be presented in a separate paper.

The CS problem may be viewed from the perspective of linear regression

$$v = B'\theta_s + n_s \tag{24}$$

where θ_s is the original basis-weight vector θ where all but the S largest coefficients are set to zero, and n_s is an error or “noise” term that accounts for the error manifested by constituting a sparse representation of the weights, θ_s ; the term n_s may also account for measurement noise, if present. The matrix B' represents B , but with only the n randomly selected rows associated with the CS measurements retained. This is a “standard” linear regression problem [11], which we solve in a Bayesian setting. In particular, we place a sparseness prior on the weights θ_s , generalizing the relevance vector machine of Tipping [30]. The generalization is manifested by assuming v , B' , θ_s and n_s are complex, rather than being real, as in [30] (and most previous CS studies).

Assume that v and n_s are of dimension n , and that θ_s is of dimension m ($n \ll m$), and that B is a known $n \times m$ complex matrix (corresponding to the n randomly selected CS measurements, in the sense discussed in [21]). Let $n_{s,i}$ represent the i th sample of n_s , $i = 1, 2, \dots, n$. The real and imaginary parts of $n_{s,i}$ are assumed drawn iid from a zero-mean Gaussian distribution with precision α_o :

$$\Re\{n_{s,i}\} \sim \mathcal{N}(0, \alpha_o^{-1}) \quad \Im\{n_{s,i}\} \sim \mathcal{N}(0, \alpha_o^{-1}), \quad iid, \quad i = 1, 2, \dots, n \tag{25}$$

The precision α_o is assumed drawn from a Gamma distribution with hyper-parameters a and b :

$$\alpha_o \sim \Gamma(a, b) \tag{26}$$

Further, the real and imaginary parts of the i th component of θ_s , respectively $\Re\{\theta_{s,i}\}$ and $\Im\{\theta_{s,i}\}$, are also drawn from a zero-mean Gaussian, now with precision α_i :

$$\Re\{\theta_{s,i}\} \sim \mathcal{N}(0, \alpha_i^{-1}) \quad \Im\{\theta_{s,i}\} \sim \mathcal{N}(0, \alpha_i^{-1}), \quad iid, \quad i = 1, 2, \dots, m \quad (27)$$

where

$$\alpha_i \sim \Gamma(c, d) \quad iid, \quad i = 1, 2, \dots, m \quad (28)$$

The hyper-parameters c and d are set such that it is highly probable that the drawn α_i will be large, implying that most $\theta_{s,i}$ are drawn from a zero-mean Gaussian with variance very close to zero. Hence, through appropriate setting of c and d (see [30] for a detailed discussion), most components of θ_s are likely to be near zero, with only a small (sparse) subset being non-zero. The likelihood function [30], wherein the observed data v is accounted for, acts to select which particular sparse representation for θ_s best fits the data (the prior may generate an infinite set of weights θ_s , each of them sparse, and the posterior defines the distribution on which θ_s are most representative of the observed data v).

The above hierarchical model is of a form for which variational Bayesian (VB) inference [31] is particularly well suited, and therefore this has been considered here. This fully Bayesian analysis provides the mean value of θ_s , as well as a measure of the associated uncertainty. This feature is particularly attractive in practical CS applications, for which the proper number of CS measurements is typically not known *a priori*, since the underlying signal u is unknown (and hence its sparseness in basis Ψ is unknown). One may continue randomly performing CS measurements in the sense discussed in [21], until the VB-inferred “error bars” are below a prescribed setting.

REFERENCES

- [1] I. Daubechies, *Ten Lectures on Wavelets*. SIAM, 1992.
- [2] S. Mallat, *A Wavelet Tour of Signal Processing*, 2nd ed. Academic Press, 1998.
- [3] A. Said and W. A. Pearlman, “A new fast and efficient image codec based on set partitioning in hierarchical trees,” *IEEE Trans. Circuits Systems for Video Technology*, vol. 6, pp. 243–250, 1996.
- [4] W. A. Pearlman, A. Islam, N. Nagaraj, and A. Said, “Efficient, low-complexity image coding with a set-partitioning embedded block coder,” *IEEE Trans. Circuits Systems Video Technology*, vol. 14, pp. 1219–1235, Nov. 2004.
- [5] E. Candès and T. Tao, “The Dantzig selector: statistical estimation when p is much larger than n ,” 2005, Preprint.

- [6] E. Candès, J. Romberg, and T. Tao, "Robust uncertainty principles: Exact signal reconstruction from highly incomplete frequency information," *IEEE Trans. Information Theory*, vol. 52, no. 2, pp. 489–509, Feb. 2006.
- [7] D. L. Donoho, "Compressed sensing," *IEEE Trans. Information Theory*, vol. 52, no. 4, pp. 1289–1306, Apr. 2006.
- [8] D. L. Donoho, Y. Tsaig, I. Drori, and J.-C. Starck, "Sparse solution of underdetermined linear equations by stagewise orthogonal matching pursuit," Mar. 2006, Preprint.
- [9] J. Haupt and R. Nowak, "Signal reconstruction from noisy random projections," *IEEE Trans. Information Theory*, vol. 52, no. 9, pp. 4036–4048, Sept. 2006.
- [10] J. A. Tropp and A. C. Gilbert, "Signal recovery from partial information via orthogonal matching pursuit," Apr. 2005, Preprint.
- [11] T. Hastie, R. Tibshirani, and J. Friedman, *The Elements of Statistical Learning*. Springer-Verlag, 2001.
- [12] D. Takhar, J. Laska, M. Wakin, M. Duarte, D. Baron, S. Sarvotham, K. Kelly, and R. Baraniuk, "A new compressive imaging camera architecture using optical-domain compression," in *Proc. of Computational Imaging IV at SPIE Electronic Imaging, San Jose, California*, 2006.
- [13] M. Wakin, J. Laska, M. Duarte, D. Baron, S. Sarvotham, D. Takhar, K. Kelly, and R. Baraniuk, "Compressive imaging for video representation and coding," in *Proc. Picture Coding Symposium (PCS), Beijing, China*, 2006.
- [14] M. Lustig, D. Donoho, and J. Pauly, "Sparse MRI: The application of compressed sensing for rapid MR imaging."
- [15] B. Zel'dovich, P. N.F., and V. Shkunov, *Principles of Phase Conjugation*. Springer-Verlag, 1985.
- [16] G. Lerosey, J. de Rosny, A. Tourin, and M. Fink, "Focusing beyond the diffraction limit with far-field time reversal," *Science*, vol. 315, p. 1120, 2007.
- [17] M. Fink, "Time reversed acoustics," *Physics Today*, vol. 50, pp. 34–40, 1997.
- [18] D. Liu, S. Vasudevan, J. Krolik, G. Bal, and L. Carin, "Electromagnetic time-reversal source localization in changing media: Experiment and analysis," *IEEE Trans. Antennas Propagation*, vol. 55, pp. 344–354, Feb. 2007.
- [19] A. Papoulis and S. U. Pillai, *Probability, Random Variables and Stochastic Processes*, 4th ed. McGraw-Hill, 2002.
- [20] G. Golden, C. Foschini, R. Valenzuela, and P. Wolniansky, "Detection algorithm and initial laboratory results using V-BLAST space-time communication architecture," *Electronic Letts.*, vol. 35, 1999.
- [21] E. Candès and J. Romberg, "Sparsity and incoherence in compressive sampling," *Inverse Problems*, vol. 23, pp. 969–985, 2007.
- [22] E. Candès and T. Tao, "Near optimal signal recovery from random projections: Universal encoding strategies?" *IEEE Trans. Information Theory*, vol. 52, no. 12, pp. 5406–5425, 2006.
- [23] M. Figueiredo, R. D. Nowak, and S. J. Wright, "Gradient projection for sparse reconstruction: Application to compressed sensing and other inverse problems," 2007, Preprint.
- [24] S. Ji, Y. Xue, and L. Carin, "Bayesian compressive sensing," Jan. 2007, Preprint.
- [25] E. Cands and J. Romberg, "Practical signal recovery from random projections," in *Wavelet Applications in Signal and Image Processing XI, Proc. SPIE Conf. 5914*, 2005.
- [26] C. Balanis, *Advanced Engineering Electromagnetics*. New York, NY: Wiley, 1989.
- [27] R. Harrington, *Field Computation by Moment Methods*. IEEE Press, 1993.
- [28] P. Blomberg, G. Papanicolaou, and H. Zhao, "Super-resolution in time-reversal acoustics," *J. Acoust. Soc. of Am.*, vol. 111, pp. 230–248, 2002.
- [29] L. Felsen and N. Marcuvitz, *Radiation and Scattering of Waves*. Piscataway, NJ: IEEE Press, 1994.

- [30] M. E. Tipping, "Sparse Bayesian learning and the relevance vector machine," *Journal of Machine Learning Research*, vol. 1, pp. 211–244, 2001.
- [31] C. M. Bishop and M. E. Tipping, "Variational relevance vector machines," in *Proc. of the 16th Conference on Uncertainty in Artificial Intelligence (UAI 16)*, 2000, pp. 46–53.